2013 American Control Conference (ACC)
Washington, DC, USA, June 17-19, 2013

Stability Control in Aerial Manipulation

Matko Orsag, Christopher Korpela, Miles Pekala, and Paul Oh

Abstract— **Aerial manipulation, grasping, and perching in small unmanned aerial vehicles (UAVs) require specific control systems to compensate for changing inertial properties. Grasped objects, external forces from terrain objects, or manipulator movements themselves may destabilize or otherwise alter the flight characteristics of small UAVs during operation resulting in undesirable outcomes. Traditional control methods that assume static mass and inertial properties must be modified to produce stable control of a quadrotor system. This paper presents work towards a control scheme to achieve dynamic stability of an aerial vehicle while under the influence of manipulators and grasped objects. A quadrotor with attached multi-degree of freedom manipulators is implemented in simulation and constructed for testing. Compensation of the inertial changes due to in-flight manipulator movements is investigated. A control scheme is developed and results are presented.**

I. Introduction

Dynamically balancing robots with arms involve challenging control problems since the vehicle's base and manipulators are often strongly coupled. The changing inertial properties of the arms, the impact of a grasped object, or environmental forces can be significant enough to warrant active reduction or compensation to maintain stability. Previous work with ground systems has shown that if vibration suppression control is not correctly handled it can lead to destabilizing effects [1]. Additionally, others have analyzed arm recovery motions to reduce the impact on a dynamically stable base vehicle [2]. Similar work with humanoids has been done involving balancing during manipulation or grasping for added stability [3].

With the focus of dynamic stability on ground-based mobile manipulators, little work has been done in aerial vehicles where arm or manipulator motions may lead to decreased stability. There have been recent attempts in aerial grasping using a 1-DOF (degree of freedom) grasper or gripper [4], [5], [6]. Other groups have introduced gimbals [7], suspended payload [8], force sensors [9], or brushes [10] attached to quadrotors or duct-fan vehicles where the manipulator is used for contact inspection. The AIRobots consortium [11] is also developing service robots for use in hazardous or unreachable locations. Previous work from the authors has produced a prototype 3-arm aerial manipulator in addition to a miniature test and evaluation quadrotor emulation system [12], [13].

Manuscript received March 15, 2013. This project was supported in part by a US NSF CRI II-New, Award # CNS-1205490, DoD Advanced Civil Schooling, U.S. Fullbright Scholarship, and the European Community Seventh Framework Programme under grant No. 285939 (ACROSS).

M. Orsag is with Faculty of Electrical Engineering and Computing, University of Zagreb, 10000 Zagreb, Croatia morsag@fer.hr

C. Korpela and P. Oh are with the Drexel Autonomous Systems Lab, Drexel Univeristy, Philadelphia, PA 19104 USA cmk325@drexel.edu, paul@coe.drexel.edu

M. Pekala is with Motile Robotics Inc., Joppa, MD 21085 USA miles.pekala@motilerobotics.com

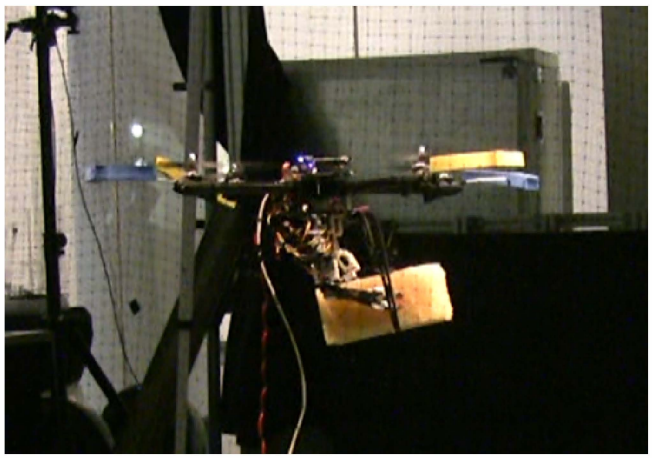

Fig. 1: MM-UAV grabbing a block

Compensating reactionary forces becomes critical and mandates a novel control architecture for both flight and arm dynamics. The reaction forces observed during arm movement and ground contact introduce destabilizing effects onto an already inherently unstable system. Recent advances in aircraft payloads and developments in light-weight arms signal a positive trend toward dexterous aerial manipulation. Payload limitations will most likely not represent the critical issue rather how arm trajectories and ground interactions produce forces and torques on the aircraft.

This paper presents a stability control scheme and model for a mobile manipulating unmanned aerial vehicle (dubbed MM-UAV). The manipulator kinematics and quadrotor model are described in Sections II and III. Stability analysis (Sec. IV) is performed on the model to develop permissible arm movements that do not violate flight stability regions. The model and control architecture is implemented in hardware (Sec. V) to characterize and compensate for reactionary forces. The aerial manipulation system presented in this paper can successfully grasp and transport various objects while maintaining stable flight.

II. Manipulator Kinematics

The manipulation structure as a whole is represented as a 'squid', a collection of serial chain manipulators in a rigid structure. The squid occupies it's own reference frame S defined with respect to the quadrotor reference frame Q. Each serial chain also possesses it's own reference frame T_0 and is defined with respect to S. Furthermore each chain

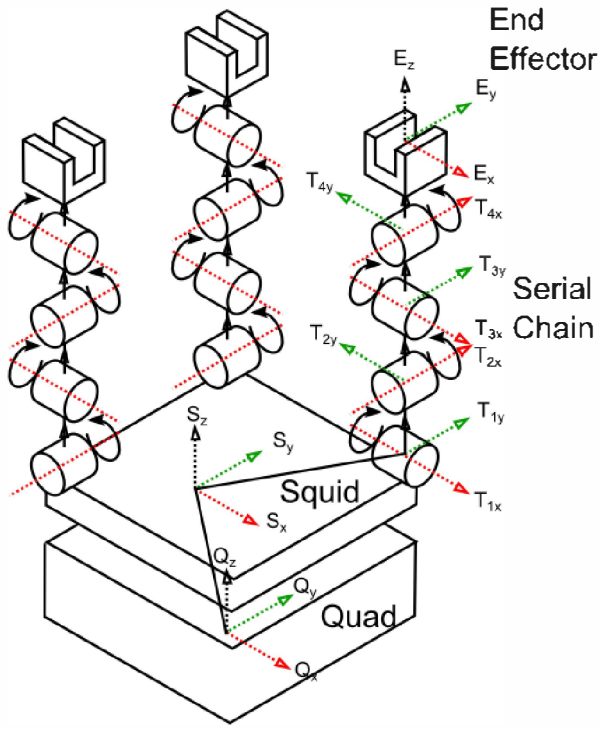

Fig. 2: Reference Frames for Manipulators

is represented by a number of frames equal to the number of links in the chain where T_l is the lth linkage in the chain. The end effector occupies it's own frame E_i for the ith chain. Using these frames we can calculate the position of the end effector from each manipulator into the world frame W. Typically the position of the quad-rotor is considered 'fixed' in W during kinematic calculations. This assumption also fixes the S in W since it is rigidly attached to the quadrotor.

Each serial chain manipulator has a number of linkages connected by revolute joints. Each joint has an axis of actuation perpendicular to the previous joint. In a four joint serial chain manipulator, this configuration provides two revolute joints in each axis as seen in Fig 2. Each link i is represented by a position $\hat{\mathbf{p}}_i = x, y, z$ in T_l, an actuation a_i, a normalized vector axis of rotation $\vec{\mathbf{r}}i$, a width, a length, and depth $\hat{\mathbf{k}}_i = w, h, d$, and a direction vector $\vec{\mathbf{v}}_i$. While this model is not the simplest, it is used for programmatic ease and model optimization may be performed if desired later. The squid possesses a position $\mathbf{p}_s$ and rotation $\mathbf{o}_s$ in Q, a vector of each chain position $\mathbf{l}_t$ in S.

Kinematics of the manipulator are basic and performed by stepping through each reference frame to the end effector of the chain. Rotation of the joint is determined by a direction cosine matrix of the actuation via the actuation axis

$$\hat{\mathbf{r}}_i = \vec{\mathbf{a}}_i \vec{\mathbf{r}} \tag{1}$$

$$\vec{\mathbf{v}}_i = \mathbf{R}(\hat{\mathbf{r}}_i)[k_i(w), 0, 0]^T \tag{2}$$

where $\hat{\mathbf{r}}_i$ is the rotation in reference to T_l. The linkage is transformed into world space by the product of previous rotations and the offset of the previous directed linkage vectors $\vec{\mathbf{v}}_{0..i-1}$

$$\hat{\mathbf{r}}_i = \mathbf{R}_{prev} \vec{\mathbf{v}}_i \tag{3}$$

$$\hat{\mathbf{p}}_i = \vec{\mathbf{v}}_{i-1} + \hat{\mathbf{p}}_{i-1} \tag{4}$$

where $\hat{\mathbf{r}}_i$ and $\hat{\mathbf{p}}_i$ are the rotation and position in reference to T. To find a set of joint angles that satisfy a particular point $\mathbf{e}$, the inverse kinematics, a simple iterative decent method is performed. In this method the Jacobian, $\mathbf{J}$, for the kinematic chain is calculated and an actuation step $\Delta\boldsymbol{\theta}$ defined by the step gain α factor and the end effector distance to the goal modifies the current serial actuations

$$\mathbf{J}(\mathbf{e}, \boldsymbol{\theta}) = \begin{bmatrix} \frac{\partial e_x}{\partial \theta_1} & \frac{\partial e_x}{\partial \theta_2} & \cdots & \frac{\partial e_x}{\partial \theta_i} \\ \frac{\partial e_y}{\partial \theta_1} & \frac{\partial e_y}{\partial \theta_2} & \cdots & \frac{\partial e_y}{\partial \theta_i} \\ \frac{\partial e_z}{\partial \theta_1} & \frac{\partial e_z}{\partial \theta_2} & \cdots & \frac{\partial e_z}{\partial \theta_i} \end{bmatrix} \tag{5}$$

$$\frac{\partial \mathbf{e}_j}{\partial \theta_i} = \vec{\mathbf{r}}i \times (\hat{\mathbf{e}} - \hat{\mathbf{p}}_i) \tag{6}$$

$$\begin{aligned} \Delta\hat{\mathbf{e}} &= \alpha(\hat{\mathbf{e}} - \hat{\mathbf{p}}_i) \\ \Delta\boldsymbol{\theta} &= \mathbf{J}^T \Delta\hat{\mathbf{e}} \\ \boldsymbol{\theta} &= \boldsymbol{\theta} + \Delta\boldsymbol{\theta} \end{aligned} \tag{7}$$

This procedure is repeated until the end effector is within a user defined 'reasonable' threshold. Superior inverse kinematics algorithms exist which are far better optimized, however this method is sufficient for the current goals.

III. Quadrotor Model

One focus of this research is to show how the manipulators influence the dynamics of the quadrotor. As such, quadrotor dynamics considered in this paper do not account for various aerodynamic effects (i.e. blade flapping, ground effect, etc.) experienced during highly dynamic flying maneuvers. Most of the vehicle's critical motions occur around hover outside of ground effect. This fact justifies a simplified mathematical model since with given speeds and maneuverability, the quadrotor experiences little to none of the previously mentioned aerodynamic effects.

A key part of quadrotor dynamics is the propulsion system torque and thrust. With no additional aerodynamic effects, propeller thrust and drag can be estimated using the NACA-standardized thrust and torque coefficients C_T (8a) and C_Q (8b). In [14], the authors measured the performance of various propellers used in UAVs. Knowing the thrust and torque coefficients of given propellers, one can easily calculate the thrust and torque of each propeller with respect to the applied voltage.

$$C_T = \frac{\|\mathbf{T}\|}{\rho n^2 D^4} \tag{8a}$$

$$C_Q = \frac{\|\mathbf{Q}\|}{\rho n^2 D^5} \tag{8b}$$

Rotor thrust and torque are marked $\mathbf{T}$ and $\mathbf{Q}$, respectively; ρ stands for air density which is assumed to be constant; $n \propto U[V]$ is the rotor speed; and D is the rotor radius. Forces and torques of each propeller are added according to

the standard quadrotor propulsion system equations as shown in (9).

$$\begin{aligned} \vec{\mathbf{F}_{tot}} &= \vec{\mathbf{T}^1} + \vec{\mathbf{T}^2} + \vec{\mathbf{T}^3} + \vec{\mathbf{T}^4} \\ \boldsymbol{\tau}_x^{tot} &= \boldsymbol{\tau}_x^2 + \boldsymbol{\tau}_x^3 - \boldsymbol{\tau}_x^1 - \boldsymbol{\tau}_x^4 \\ \boldsymbol{\tau}_y^{tot} &= \boldsymbol{\tau}_y^3 + \boldsymbol{\tau}_y^4 - \boldsymbol{\tau}_y^1 - \boldsymbol{\tau}_y^2 \\ \boldsymbol{\tau}_z^{tot} &= \boldsymbol{\tau}_z^2 + \boldsymbol{\tau}_z^4 - \boldsymbol{\tau}_z^1 - \boldsymbol{\tau}_z^3 \end{aligned} \tag{9}$$

Dynamics of brushless DC motors used on the aircraft proved to have an important impact in aircraft stability and cannot be omitted from the MM-UAV model. Off the shelf electronic speed controllers are used to power and control the motors, which makes it impossible to devise a complete model for the motors. Therefore, a simplified 1st order PT1 dynamic model is used.

Considering simplified aerodynamic conditions, propellers simply produce thrust forces $\vec{\mathbf{T}^i}$ as shown in (8a). Summing them all together gives the total aircraft thrust. Each propeller torque $\vec{\boldsymbol{\tau}}^i$, in contrast, has two components, one coming from the actual propeller drag (8b), and the other due to the displacement of the propeller from the COG (center of gravity).

$$\vec{\boldsymbol{\tau}}^i = \vec{\mathbf{Q}}^i + \Delta\vec{\mathbf{R}}_T^i \times \vec{\mathbf{T}}^i \tag{10}$$

IV. Stability Analysis

Given quadrotor body dynamics and manipulator kinematics, a simplified arm model is utilized to establish stability criteria for the complete system. Much of the previous work in quadrotor flight and stability assumes the geometric center and quadrotor center of mass are coincident. In our model as shown in Figs. 3a and 3b, the quadrotor center of mass $\mathbf{Q}_{CM}$ is shown offset downward in the z direction due to the mass of the arms. Further, the overall center of mass, **CM**, shifts based on the joint angles of the two shoulder joints.

Prior work in aircraft stability analysis has measured center of mass offsets based on the load mass while ignoring affects from the gripper [4], [5]. In this work, the 4-DOF arms and end-effectors introduce a significant increase in payload and disturbance to the dynamics and therefore cannot be neglected.

A. Simplified Kinematics

The simplified kinematics approach shown in Figs. 3a and 3b divides the system into 4 parts: quadrotor body, arms A and B, and added payload D (i.e. foam block or balsa stick). We only observe the movements of the second joints q_A^2 and q_B^2 where the remainder of the arm joints remain fixed. This simplification allows us to view the arms as links of length C and mass $m_A = m_B$, and corresponding moments of inertia. In the simplified approach, each element's moment of inertia is written as a diagonal tensor:

$$\mathbf{I} = {\mathbf{R}_{GC}^X}^T \begin{bmatrix} I_{xx} & 0 & 0 \\ 0 & I_{yy} & 0 \\ 0 & 0 & I_{zz} \end{bmatrix} \mathbf{R}_{GC}^X \tag{11}$$

with transformation matrix $\mathbf{R}_{GC}^X$ that transforms the moment of inertia into a geometric center coordinate system. Each element, except the quadrotor which is calculated separately, is modeled as a prismatic joint. Therefore, the key equation for the principal axis moment of inertia is simplified to:

$$I_{xx} = \frac{m{l_x}^2}{12} \tag{12}$$

The longer the link l_x in any direction x and the more mass m it has, the larger the impact it has on the overall system dynamics. Key aspects observed are the changes in roll and pitch angle dynamics. This analysis could later be easily applied to yaw angle stability. For both manipulation tasks, arms A and B move together. The first item is the varying center of mass vector position:

$$\mathbf{CM} = \frac{\sum \mathbf{X}_{cm} m_X}{\sum m_X} \tag{13}$$

where $\mathbf{X}$ stands for each element of the model; notations Q, A, B and D mark quadrotor, arms A, B, and added payload D; m_X are respective element masses. Vectors $\mathbf{A}_{cm}, \mathbf{B}_{cm}$ and $\mathbf{D}_{cm}$ change as joints q_A^1, q_B^1, and q_A^2, q_B^2 move. Analyzing the two situations separately, the equations for these vectors can be derived:

$$\mathbf{A}_{cm} = -d \cdot \hat{\mathbf{x}} + [Csin(q)]\,\hat{\mathbf{y}} + [L_2 + Ccos\,(q)]\,\hat{\mathbf{z}} \tag{14a}$$

$$\mathbf{B}_{cm} = d \cdot \hat{\mathbf{x}} + [Csin(q)]\,\hat{\mathbf{y}} + [L_2 + Ccos\,(q)]\,\hat{\mathbf{z}} \tag{14b}$$

$$\mathbf{D}_{cm} = 2C \cdot sin(q)\hat{\mathbf{y}} + [L + 2Ccos\,(q)]\,\hat{\mathbf{z}} \tag{14c}$$

with constant dimensions d, L and C marked in Figs. 3a and 3b.

Using the Parallel axis theorem, one can easily calculate the overall moment of inertia $\mathbf{I}_{CM}$ that changes as the joints move. Further, it varies depending on the payload size and mass:

$$\begin{aligned} \mathbf{I}_{CM} &= \mathbf{I}_Q + \mathbf{I}_A + \mathbf{I}_B + \mathbf{I}_D \\ &\quad + m_Q \Delta\tilde{\mathbf{Q}}^2 + m_A \Delta\tilde{\mathbf{A}}^2 + m_B \Delta\tilde{\mathbf{B}}^2 + m_D \Delta\tilde{\mathbf{D}}^2 \end{aligned} \tag{15}$$

where $\Delta\tilde{\mathbf{Q}}, \Delta\tilde{\mathbf{A}}$, $\Delta\tilde{\mathbf{B}}$ and $\Delta\tilde{\mathbf{D}}$ represent the center of mass of each body with respect to the center of mass frame, written in the skew matrix form; **CM** and $\mathbf{I}_Q, \mathbf{I}_A, \mathbf{I}_B$, and $\mathbf{I}_D$ are corresponding moments of inertia in each element's center of mass. Each vector distance $\Delta\mathbf{X}$ is calculated as the difference between the element centroid and the overall centroid **CM** (13) with respect to the GC, $\Delta\ \mathbf{X} = \mathbf{X}_{CM} - \mathbf{CM}$.

Final equations for the CM moment of inertia are shown graphically in Fig. 4. The images are plotted relative to the quadrotor moment of inertia $\mathbf{I}_Q$. Although the effects of both payloads are similar, there are a few substantial differences. The two plots at the top of the figure show how the moment of inertia changes due to joint angle changes and stick length increase. Both plots show an increase in the moment of inertia as the arms move from a horizontal to vertical position. An increase in stick length also adds to the overall moment of inertia. The stick is modeled as an infinitesimally thin prismatic joint and therefore has only one principal axis greater than zero (i.e. the one pointing at its length). Referring back to (12), it is easy to show how a linear increase in stick length has a cubic relation to moment of inertia increase ($I_{CM} \sim L_S$). This effect is shown in Fig. 4d.

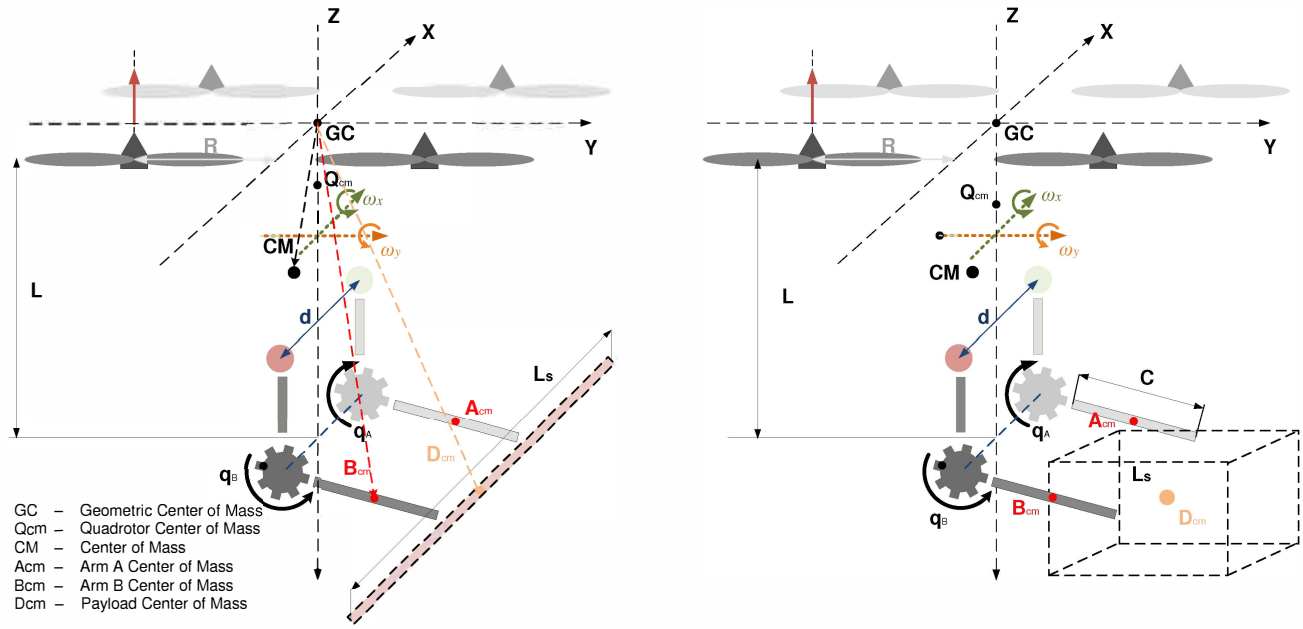

(a) Carrying a stick (b) Box-type object carrying

Fig. 3: Simplified dynamic model in two basic manipulation operations.

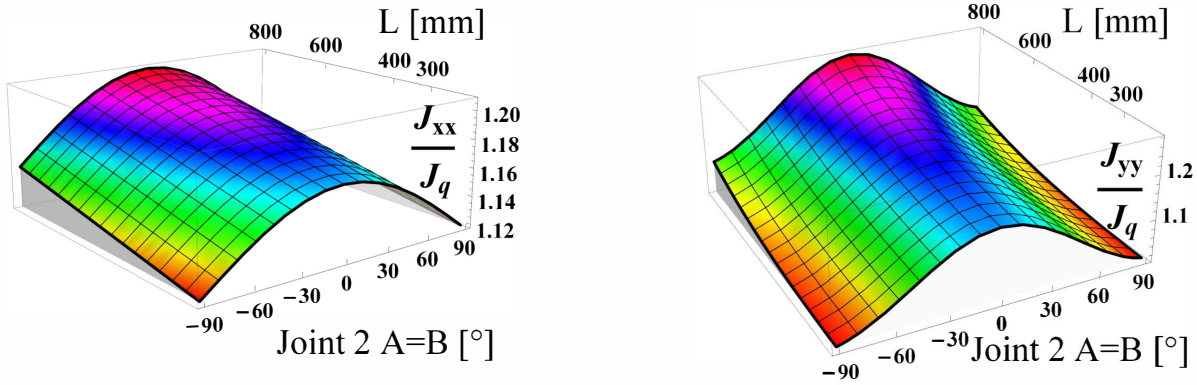

(a) Stick transport - I_{xx} with respect to stick length and joint angles (b) Stick transport - I_{yy} with respect to stick length and joint angles

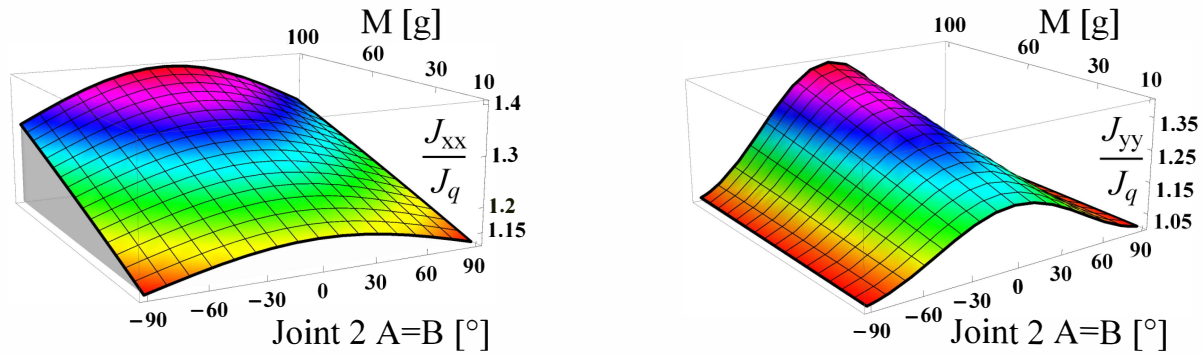

(c) Box transport - I_{xx} with respect to stick length and joint angles (d) Box transport - I_{yy} with respect to stick length and joint angles

Fig. 4: Moments of inertia variations in two basic manipulation tasks.

The lower two plots in Fig. 4 show moment of inertia change as the mass of the added foam box payload increases. This is also shown together with joint position changes where the previous effects are observed but to a greater degree. In these figures, the box size is kept constant and only its mass varies. A linear relation between box object mass and overall moment of inertia is shown in these figures. These plots show how simple manipulation tasks can change the total moment of inertia, causing potential stability problems, which will be analyzed in the following section.

B. Angle Control Stability

Control of the quadrotor body is achieved through PI-D control shown in Fig. 5. This form of PID control was chosen because it eliminates potential damages to the actuators that can usually be experienced when leading the control difference directly through the derivation channel [15]. In order to analyze the stability of the system, one needs to know the varying parameters in the control loop. The disturbance caused from the Euler equation component $\omega_y\omega_z(I_{yy}-I_{zz})$ affects the behavior of the control loop, but not its stability and therefore will not be considered in this analysis. The major factor that affects the stability of the aircraft is the moment of inertia $J = I_{xx}, I_{yy}$. Mathematical formalisms that describe the variations in the moment of inertia was given in Sec. IV-A. The transfer function of the angle control loop in Fig. 5 can easily be derived (16). Similarly as in [5], the stability conditions are applied to its 4th order characteristic polynomial $a_4s^4+a_3s^3+a_2s^2+a_1s+a_0$, where the 4th order dynamic system includes both the dynamics of the aircraft and motor dynamics [16].

$$G_{\alpha_{CL}} = \frac{\frac{K_DK_m}{K_iT_mJ}\left(\frac{K_p}{K_i}s+1\right)}{s^4+\frac{1}{T_m}s^3+\frac{K_DK_m}{T_mJ}s^2+\frac{K_dK_mK_p}{T_mJ}s+\frac{K_pK_mK_i}{T_mJ}} \tag{16}$$

Coefficients K_D, K_p and K_i are PI-D respective gains and K_m and T_m represent propulsion system gain and the motor time constant. If we apply the Routh-Hurwitz stability criteria, it is possible to derive the analytical equations for stability conditions. The necessary system stability conditions require that all coefficients be positive and that inequalities in (17) are satisfied. Stability criterion (17) shows that, due to the dynamics introduced from the motors (i.e. T_m), the proportional control K_p can drive the system unstable. In fact, only the derivative control K_d has the sole purpose of stabilizing the system. This shows how the motor dynamics cannot be neglected when analyzing MM-UAV stability.

$$\frac{K_dK_mK_p}{K_i}\left(1-T_mK_p\right) > J \tag{17a}$$

$$K_dK_m\left(1-T_mK_p\right) > 0 \tag{17b}$$

Moreover, the angle control loop in Fig. 5 can be observed as a cascade system, where the K_D gain serves as an inner loop controller. This approach enables tuning the PI-D controller in two separate steps (i.e. rotation speed and angle loop). After closing the speed loop, the inner loop transfer function takes the standard 2nd order transfer function form:

$$G_{\omega_{CL}} = \frac{1}{1+\frac{J}{K_DK_m}s+\frac{JT_m}{K_DK_m}s^2} \tag{18}$$

It can further be shown that the equations for the system's natural frequency ω_n and damping ratio ζ are:

$$\omega_n = \sqrt{\frac{K_DK_m}{JT_m}} \tag{19a}$$

$$\zeta = \frac{1}{2}\sqrt{\frac{J}{K_DK_mT_m}} \tag{19b}$$

While from (17) follows that a smaller moment of inertia increases the system stability, (19) shows that smaller moments of inertia cause oscillations in the inner loop. While that is not a problem in this analysis, in the actual implementation, where a discrete form and input limits are used, the amplitude and frequency of these oscillations can cause serious problems and stability issues. The amplitude can causes problems when faced with control inputs limits (i.e. $12V$) and the frequency is of concern when it surpasses the sampling frequencies. Smaller moments of inertia produce higher frequencies and smaller damping ratios thus can decrease the stability in multiple ways.

V. Experimental Results

A. Test Setup

The test vehicle is constructed using a low-cost quadrotor aircraft (GAUI 500X) and two manipulator arms. The quadrotor uses four equally positioned 960 kV brushless motors equipped with 10 inch propellers to provide lift and maneuverability. The vehicle diameter is 500mm and the aircraft is capable of lifting objects below 500g. A landing gear system, originally designed for a pan-tilt camera, has been modified to provide an unobstructed workspace for the manipulators. An off-the-shelf IMU (inertial measurement unit) fused with motion capture data is used to control the yaw, pitch, and roll of the quadrotor. Indirect Kalman filtering is used to combine gyroscopic sensor data and motion capture visual feedback. Low-level control is implemented on an Arducopter board that runs Kalman filtering and a PI-D controller loop with a $50Hz$ sample rate. Motion capture is based on vision markers placed just above the center of mass of the vehicle. An operator controls both the quadrotor and arms using a joystick that provides position control of the air vehicle and joint control of the servos. A ROS-based PC program routes available motion capture data (i.e. x, y, z position and speed) and joystick data to the Arducopter board using rosserial. The motion capture system used in this research is based on 18 V100:R2 OptiTrack cameras connected to a separate PC running Arena Software.

B. Flight Tests

Following lift-off under manual control, the autopilot is enabled. The operator can move the aircraft to achieve a suitable hover location in addition to changing arms from a

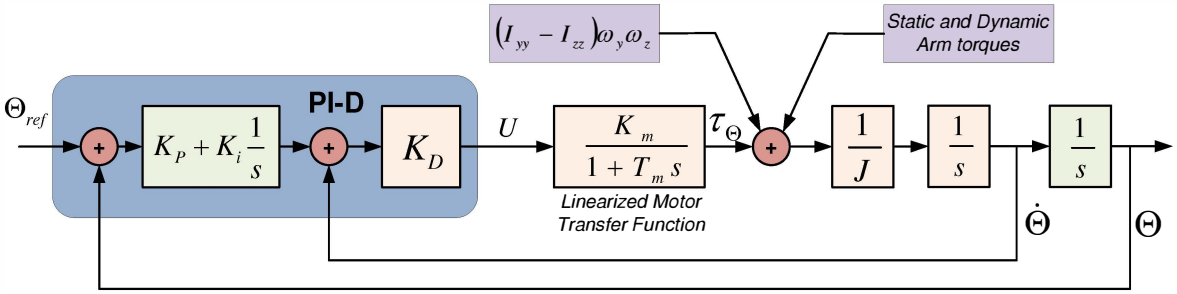

Fig. 5: Attitude Control Loop [16]

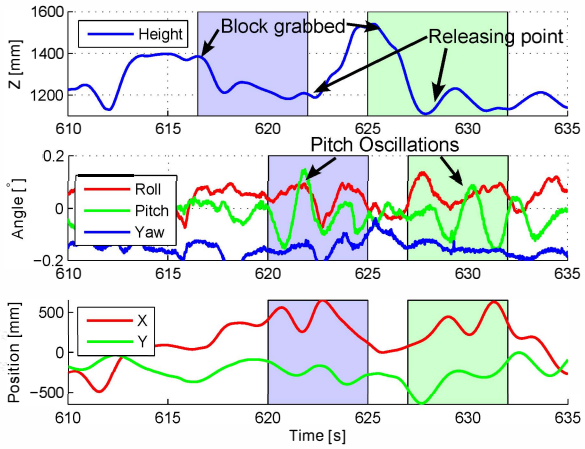

Fig. 6: Two Grab and Drop Experiments: Notice the large pitch oscillations and x displacement following the grab (t = 617s and 625s) [16].

stow position to grab posture. Fig. 6 illustrates a grab and drop experiment using a foam block as shown in Fig. 1. The first block grab test is highlighted in blue and the second test is highlighted in green. The arms are used to clamp the block, the aircraft moves to a desired location, and the block is released. In this experiment, when the block is grabbed, the vehicle drops in altitude and shows large pitch oscillations and displacement along the x axis. Once the block is released, the vehicle stabilizes and gains in altitude.

VI. Conclusions

In this paper a control methodology for a multi-arm manipulating aerial vehicle is presented. The system kinematics have been applied to our controller implementation to compensate for reactionary forces during arm movement. Through stability analysis, we have identified manipulator joint positions that ensure flight stability for a simple PI-D controller. Flight tests confirm the kinematic model and controller for the system. In the future, we plan to test different adaptive and robust control techniques in order to achieve greater flight stability and more dexterous manipulation.

References

[1] T. Wimbock, D. Nenchev, A. Albu-Schaffer, and G. Hirzinger, "Experimental study on dynamic reactionless motions with dlr's humanoid robot justin," in *Proc. IEEE/RSJ Int. Conf. Intelligent Robots and Systems IROS 2009*, 2009, pp. 5481–5486.

[2] S. Kuindersma, R. Grupen, and A. Barto, "Learning dynamic arm motions for postural recovery," in *Humanoid Robots (Humanoids), 2011 11th IEEE-RAS International Conference on*, oct. 2011, pp. 7 –12.

[3] K. Harada, S. Kajita, K. Kaneko, and H. Hirukawa, "Dynamics and balance of a humanoid robot during manipulation tasks," *IEEE Trans. Robot.*, vol. 22, no. 3, pp. 568–575, 2006.

[4] D. Mellinger, Q. Lindsey, M. Shomin, and V. Kumar, "Design, modeling, estimation and control for aerial grasping and manipulation," in *Proc. IEEE/RSJ Int Intelligent Robots and Systems (IROS) Conf*, 2011, pp. 2668–2673.

[5] P. E. I. Pounds, D. R. Bersak, and A. M. Dollar, "Grasping from the air: Hovering capture and load stability," in *Proc. IEEE Int Robotics and Automation (ICRA) Conf*, 2011, pp. 2491–2498.

[6] V. Ghadiok, J. Goldin, and W. Ren, "Autonomous indoor aerial gripping using a quadrotor," in *Intelligent Robots and Systems (IROS), 2011 IEEE/RSJ International Conference on*, sept. 2011, pp. 4645 – 4651.

[7] A. Keemink, M. Fumagalli, S. Stramigioli, and R. Carloni, "Mechanical design of a manipulation system for unmanned aerial vehicles," in *Robotics and Automation (ICRA), 2012 IEEE International Conference on*, may 2012, pp. 3147 –3152.

[8] I. Palunko, R. Fierro, and P. Cruz, "Trajectory generation for swing-free maneuvers of a quadrotor with suspended payload: A dynamic programming approach," in *Robotics and Automation (ICRA), 2012 IEEE International Conference on*, may 2012, pp. 2691 –2697.

[9] S. Bellens, J. De Schutter, and H. Bruyninckx, "A hybrid pose / wrench control framework for quadrotor helicopters," in *Robotics and Automation (ICRA), 2012 IEEE International Conference on*, may 2012, pp. 2269 –2274.

[10] A. Albers, S. Trautmann, T. Howard, T. A. Nguyen, M. Frietsch, and C. Sauter, "Semi-autonomous flying robot for physical interaction with environment," in *Robotics Automation and Mechatronics (RAM), 2010 IEEE Conference on*, june 2010, pp. 441 –446.

[11] www.airobots.eu.

[12] M. Orsag, C. Korpela, and P. Oh, "Modeling and control of MM-UAV: Mobile manipulating unmanned aerial vehicle," *Journal of Intelligent and Robotic Systems*, vol. 69, pp. 227–240, 2013.

[13] C. Korpela, M. Orsag, T. Danko, B. Kobe, C. McNeil, R. Pisch, and P. Oh, "Flight stability in aerial redundant manipulators," in *Proc. IEEE Int Robotics and Automation (ICRA) Conf*, 2012.

[14] M. P. Merchant, "Propeller performance measurement for low Reynolds number unmanned aerial vehicle applications," 2004.

[15] N. Miskovic, Z. Vukic, M. Bibuli, M. Caccia, and G. Bruzzone, "Marine vehicles' line following controller tuning through self-oscillation experiments," in *Proceedings of the 2009 17th Mediterranean Conference on Control and Automation*, ser. MED '09, 2009, pp. 916–921.

[16] C. Korpela, M. Orsag, M. Pekala, and P. Oh, "Dynamic stability of a mobile manipulating unmanned aerial vehicle," in *Proc. IEEE Int Robotics and Automation (ICRA) Conf*, 2013, To Appear.